

**Concrete-ice abrasion**

**Wear, coefficient of friction and ice consumption**

Shamsutdinova, Guzel; Hendriks, Max A.N.; Jacobsen, Stefan

**DOI**

[10.1016/j.wear.2018.09.007](https://doi.org/10.1016/j.wear.2018.09.007)

**Publication date**

2018

**Document Version**

Accepted author manuscript

**Published in**

Wear

**Citation (APA)**

Shamsutdinova, G., Hendriks, M. A. N., & Jacobsen, S. (2018). Concrete-ice abrasion: Wear, coefficient of friction and ice consumption. *Wear*, 416–417, 27-35. <https://doi.org/10.1016/j.wear.2018.09.007>

**Important note**

To cite this publication, please use the final published version (if applicable).  
Please check the document version above.

**Copyright**

Other than for strictly personal use, it is not permitted to download, forward or distribute the text or part of it, without the consent of the author(s) and/or copyright holder(s), unless the work is under an open content license such as Creative Commons.

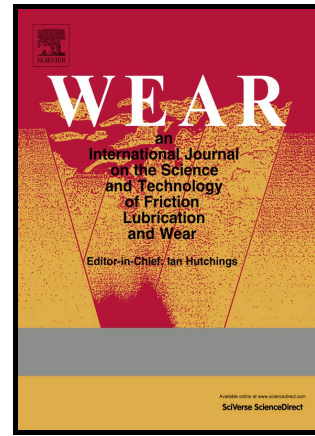
**Takedown policy**

Please contact us and provide details if you believe this document breaches copyrights.  
We will remove access to the work immediately and investigate your claim.

# Author's Accepted Manuscript

Concrete-ice abrasion: wear, coefficient of friction and ice consumption

Guzel Shamsutdinova, Max A.N. Hendriks, Stefan Jacobsen



[www.elsevier.com/locate/wear](http://www.elsevier.com/locate/wear)

PII: S0043-1648(18)30747-6  
DOI: <https://doi.org/10.1016/j.wear.2018.09.007>  
Reference: WEA102506

To appear in: *Wear*

Received date: 29 June 2018  
Revised date: 7 September 2018  
Accepted date: 11 September 2018

Cite this article as: Guzel Shamsutdinova, Max A.N. Hendriks and Stefan Jacobsen, Concrete-ice abrasion: wear, coefficient of friction and ice consumption, *Wear*, <https://doi.org/10.1016/j.wear.2018.09.007>

This is a PDF file of an unedited manuscript that has been accepted for publication. As a service to our customers we are providing this early version of the manuscript. The manuscript will undergo copyediting, typesetting, and review of the resulting galley proof before it is published in its final citable form. Please note that during the production process errors may be discovered which could affect the content, and all legal disclaimers that apply to the journal pertain.

# Concrete-ice abrasion: wear, coefficient of friction and ice consumption

Guzel Shamsutdinova<sup>1</sup>, Max A.N. Hendriks<sup>1,2</sup> and Stefan Jacobsen<sup>1</sup>

<sup>1</sup>Norwegian University of Science and Technology, Department of Structural Engineering, Richard Birkelandsvei 1A, 7491 Trondheim, Norway

<sup>2</sup>Delft University of Technology, Faculty of Civil Engineering and Geosciences, Stevinweg 1, 2628

CN Delft, The Netherlands

guzel.shamsutdinova@ntnu.no

max.hendriks@ntnu.no

stefan.jacobsen@ntnu.no

## Abstract

Concrete structures in the Arctic offshore are often exposed to drifting ice causing abrasion of concrete surfaces. This paper presents the results of a laboratory study of concrete-ice abrasion. The sawn concrete surfaces (two high-performance concrete mixes and one light weight mix of concrete) were exposed to sliding fresh-water ice under 1 MPa pressure for 3 km of sliding distance. The effect of concrete compressive strength, ice consumption, and the coefficient of friction on abrasion was studied simultaneously. The results show a low abrasion of concrete, the maximum abrasion depth (0.35 mm) after 3 km of sliding test was found for the concrete samples with the lowest compressive strength. All tests showed a severe-to-mild wear transition, with the maximum wear rate in the first sliding kilometre. The

coefficient of friction was high when ice consumption was high due to ice spallation and pulverization, whereas the coefficient of friction was not directly correlated to the wear. The wear or consumption of the ice (abrasive) was in the order of 30000 – 100000 times that of concrete despite of its strength and stiffness 1 – 10 times lower than that of concrete.

*Keywords:* Concrete, ice, abrasion, experiments, friction.

## 1. Introduction

The concrete-ice abrasion process has been studied for the last 30 years, and can be defined as the surface degradation of concrete structures due to interaction with drifting ice floes. The topic is especially relevant for gravity-based structures in the arctic offshore, where there is limited access to service structures, which are supposed to be able to withstand all kinds of severe environmental conditions for at least 40 years according to typical basic design requirements. In practice, the service life actually required may be substantially longer. Moreover, the degradation of concrete surfaces on a meso-scale can facilitate or initiate other degradation mechanisms, such as reinforcement corrosion, cracking, chemical and frost attack, and so on. Several research groups have therefore studied this topic in both laboratory experiments [1–6] and field observations [1, 7–9], with a view to controlling and preventing concrete ice abrasion. A major difficulty in service life modelling and prediction is that the wear mechanism involved in this process has not yet been precisely described.

Concrete-ice abrasion can be in the order of millimetres of concrete depth per year. The collision of an ice floe with a concrete structure causes various kinds of interaction. The structure's geometry, the ice load conditions and ice properties affect the nature and magnitude of the global load [10]. Concrete-ice abrasion is a result of local behaviour at the concrete surface under ice exposure by impact or sliding or both, where contact interaction between the asperities of the ice and the concrete surface seems to affect to the abrasion.

Wear is a phenomenon sensitive to many parameters, and it is usually hard to distinguish only one mechanism. Intuitively, concrete-ice abrasion can be seen as a mechanical type of wear. To be more specific, we will focus on the abrasive mode. Abrasive wear is the fracture or deformation of brittle or ductile materials respectively. Since concrete is a brittle material, two mechanisms of abrasive wear can be relevant: micro-fracture and the pull-out of individual grains.

Micro-fracture happens in brittle materials due to the scratching of a surface with a hard asperities, whereas wear grooves are observed in ductile materials. The grain pull-out mechanism is also relevant for concrete. As a composite material, concrete has low tensile strength compared to its compressive strength and relatively weak joints between the grains (the interfacial transition zone, ITZ), and entire grains can come loose as wear debris. The protrusion of coarse concrete aggregates observed by the authors in previous research [11] is evidence of this, because it means that the cement paste with fine aggregates (where the particle size is less than, say, 0.1 mm) was worn away around the coarse aggregates.

Stress concentrations around inhomogeneities can cause micro-crack initiation, and their further convergence can lead to wear. The physics of this kind of wear is crack nucleation and propagation with brittle fracture as the dominant wear process.

A recent review [12] proposed three mechanisms of concrete degradation that can be addressed to micro-crack initiation: high concrete tensile stress from ice asperity in contact with the concrete due to its low tensile strength compared to the compressive strength of confined ice; water pressed into cracks with wet ice-collision expanding these cracks; and three-body wear by sharp concrete particles between ice and concrete surfaces. In the latter case, the wear particles can be trapped by or embedded in ice, and then it is considered to be two-body wear [13].

The most common method for studying concrete-ice abrasion is through laboratory experiments. Laboratory studies typically give wear in the order of 0.1–1.0 mm of concrete per km of ice-sliding distance depending on material and exposure parameters. The method used in most of these experiments has been sliding tests, either with normally loaded ice specimens on a concrete surface or vice versa. Ideally, as many relevant load and response parameters as possible should be simultaneously controlled and measured during such wear tests: temperatures, loads, movements, wear of ice and concrete, etc. The accuracy of each individual measurement might be limited by the resources available. This research was part of an experimental study of concrete-ice abrasion in which a large number of parameters were investigated by the quantitative analysis of correlations between any parameters that might influence concrete-ice abrasion.

The scope of this research was to measure ice consumption, ice pressure, and the friction between ice and realistic high-performance concrete (HPC), and to study the relationship between these three quantities and the resulting concrete-ice abrasion. Ice consumption is a quantitative parameter of ice fracture mode, which is expected to have an effect on the wear process. For this purpose, we used the sawn surfaces of three different concrete mixes (B75, B85, and LB60) in contact with

sliding fresh-water ice in an instrumented wear measurement set-up with feedback controlled ice loading and high-frequency logging of load and response parameters.

## 2. Experiment

The experimental study included the above-mentioned simulation of concrete-ice sliding followed by measurement of abrasion wear. The contact materials and experimental method are described below. More detailed information about the equipment and set-up can be found in a recent paper [11].

### 2.1. Concrete

The tests were carried out for three different concrete mixes, with both normal and lightweight aggregates. The concrete samples were made of Norcem Anlegg cement (Portland cement CEM I 52.5 N), with 2% Elkem silica fume (grade 940 Undensified) substitution. The fillers were fine aggregate (Årdal, 0-8 mm grain size) and coarse aggregate of normal weight (Årdal, 8-16 mm grain size). The rock-mineral composition are: feldspathic rock/ feldspar particles 47%; granite 40%; dark rock 6%; quartzite, coarse grained/ quartz particles 5%; quartz rich rock 1%; mylonite/ cataclasite 1% [14]. The light weight concrete had light weight coarse aggregate (Stalite ½" and ¾" grain size). The superplasticizing admixture Dynamon SX-23 from Mapei was used to achieve the target fresh concrete workability.

The fresh concrete properties were determined in accordance with EN 12350, part 2 (slump measure), part 6 (density), and part 7 (air content) approximately 10

min after water addition [15]. The slump spread was measured as the diameter of the collapsed slump cone. The samples were classified as B75, B85 and LB60 in accordance with NS-EN 206:2013+NA:2014 [16]. The results are given in Table 1.

**Table 1** Concrete properties of tested mixes.

	<b>B75</b>	<b>B85</b>	<b>LB60</b>
W/(C+2S)*	0.42	0.38	0.40
Density, kg/m <sup>3</sup>	2455	2470	1905
Air content, %	0.9	1.0	6.7
Slump measure, mm	200	200	195
Slump spread measure, mm	420	435	410
28 days compressive strength (cube), MPa	90.0	100.4	69.1

\*where W, C and S are the free water, cement and silica fume powder (%wt)

The concrete samples used for the concrete-ice abrasion test were miniature slabs measuring 100x310 mm and 50 mm high, which were cured in water at +20°C for 11 months before the experiments. The development of the concrete compressive strength over the curing time is plotted in Fig. 1.

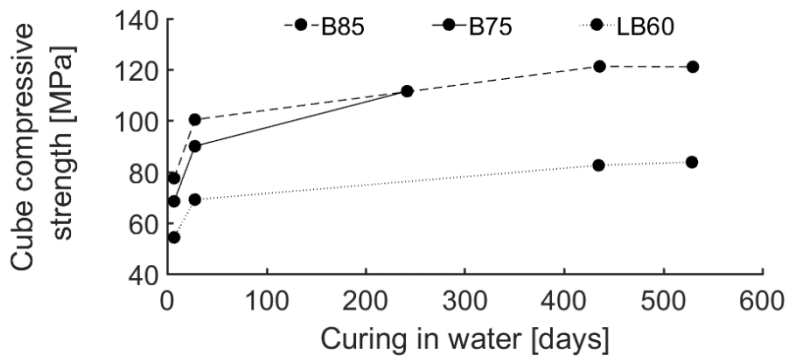


**Fig. 1.** The concrete compressive strength development curve.

## 2.2. Ice

Our abrasion machine is designed for fresh-water cylindrical ice samples with a diameter of 73.4 mm and a height of 180 mm. This substitution of fresh-water ice for seawater ice was made for two reasons. Firstly, seawater ice has complicated mechanical properties and can also involve additional parameters, such as salt, affecting the degradation of concrete. Secondly, fresh-water ice is less aggressive for the test machine. Also other researchers used fresh-water ice for sliding tests [4–6]. We have developed a simple method for preparing fresh water ice with a minimum number of air voids. The moulds for making ice are made of POM and are insulated with expanded polystyrene on the sides and bottom, resulting in unidirectional freezing. The ice preparation procedure has been described in detail in a recent paper [11].

The ice density was measured by hydrostatic weighing in kerosene [17] at  $-10$  °C. The average ice density (measured for 11 samples) was  $917.0 \text{ kg/m}^3$  for the part of the ice that is worn during the test (80 mm). The theoretical density of pure ice at  $-10$  °C is  $917.98 \text{ kg/m}^3$  [18], which means our ice samples had a porosity of 0.1%.

The ice porosity was also calculated using a method based on X-ray micro-computed tomography [19]. The results gave 0.0033% porosity for the part of the ice sample that is worn during the test (80 mm). Both methods showed a very low porosity, indicating that our ice samples were practically free of air-voids. It allowed us to use reproducible ice and neglect the porosity effect. In this way, however, we also neglected that in sea ice porosity can vary within a wide range: 2–40% depending on ice age, ice thickness and snow cover that gives sea ice a layered structure with different properties. Sea ice porosity has a great effect on its mechanical properties: high porosity decreases stiffness and strength [20]. The grain size was measured as an area fraction based on the 2D image of a thin section of

ice across the sample approximately 30 mm above the contact between ice and concrete. This showed the average 2D size of ice grains was 78 mm<sup>2</sup>.

### 2.3. Concrete-ice abrasion lab

The concrete-ice abrasion lab comprises a cold room with the abrasion machine for simulation of exposure to ice, moulds and two freezers for making ice samples, and a laser scanner for detailed measurement of concrete surfaces.

The experimental simulation of the concrete-ice abrasion process has several limitations: fresh-water ice without confinement by an ice field and moderate pressure (1 MPa), temperature (-10 °C) and duration or ice-sliding distance (3 km) of experiment. Furthermore, we use perpendicular sliding interaction back and forth only, whereas in reality the attack angle can vary depending on the drift direction. For sea ice, there will also be effects of seawater current and the ice-concrete contact will to a large extent be submerged in seawater with all types of contact varying from parallel sliding to normal impacting.

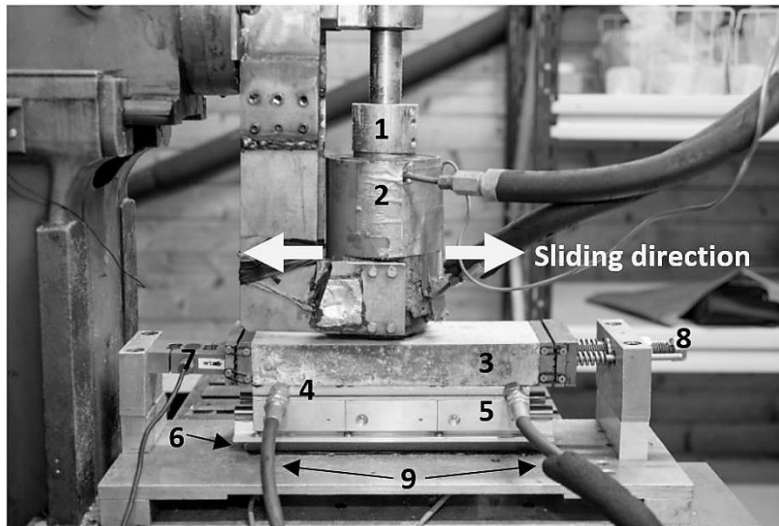
The abrasion machine makes the ice sample in the holder move in repeated horizontal sliding movements back and forth, as shown in Fig. 2. The horizontal stroke length of the machine is constant at 200 mm. The average velocity is 0.16 m/s. A vertical piston continuously pushes the ice sample against the concrete surface with a controlled load. A National Instruments programmed feedback system keeps the vertical action loading on the ice constant while the ice is moving back and forth via topside load sensors, and a servo engine controlled by a feedback system programmed in National Instruments LabView. There is a moderate cycling fluctuation of the ice pressure, which is related to the position of the ice sample and

the accuracy of the feedback system. At target pressure 1 MPa the standard deviation is 0.07 MPa. The vertical reaction force is measured via two underside load cells supporting the concrete sample. The concrete sample is positioned on a linear sliding bearing with a very low coefficient of friction (0.0015-0.005) and fixed with a pre-stressing screw on one side and a horizontal load cell on the other.

The concrete-ice abrasion lab is kept at an average temperature of  $-10\text{ }^{\circ}\text{C}$ . The temperature of the concrete sample is controlled through the aluminium heating plate between the sliding bearing and the sample. The heating plate prevents icing on the concrete surface. The heating plate has a channel inside, connected at both ends to a controlled temperature liquid (alcohol) circulator. The temperature of the concrete surface during the test is approximately  $-2\text{ }^{\circ}\text{C}$  (measured with infrared thermometer). Since a major part of contact between sea ice floe and structure is below the water level, due to the ice density, and the seawater temperature is approximately  $-2\text{ }^{\circ}\text{C}$ , we assume that temperature conditions are not too far away from real sea ice temperature conditions.

The outputs of the test include: time, position, horizontal and vertical load responses (logged at 500 Hz), and total sliding distance, ice consumption, number of cycles, and temperature (logged at 0.17 Hz).

The laser measurement of the concrete surface was carried out for 300 profiles per sample. The laser sensor measured the height of each profile on the concrete surface with a repeatability of  $10\text{ }\mu\text{m}$ , and a measuring point distance of  $50\text{ }\mu\text{m}$ . The outputs comprise the surface heights, which are transformed into a matrix of surface heights with  $1900 \times 300$  points. More details on the laser scanner are given in [11].



- |                                  |   |
|----------------------------------|---|
| 1 – Piston                       | 6 – Vertical load cells (invisible,<br>under the linear sliding system) |
| 2 – Ice sample inside the holder | 7 – Horizontal load cell  |
| 3 – Concrete sample              | 8 – Prestressing screw  |
| 4 – Aluminium heating plate      | 9 – Inlet and outlet of heating liquid                                  |
| 5 – Linear sliding system        |   |

**Fig. 2.** The concrete-ice abrasion machine.

#### 2.4. Exposure Conditions

The concrete samples were tested in sliding contact with ice and under a nominal ice pressure of 1 MPa. The surrounding air temperature was  $-10\text{ }^{\circ}\text{C}$ . Each concrete sample was tested for an effective sliding distance of 3 km. The concrete surfaces were evaluated with the laser scanner before the test and after each kilometre of effective sliding distance.

### 3. Results and Discussion

The results of the tests on sawn surfaces of the three different concrete mixes (B75, B85, and LB60) include: the abrasion of the concrete surface, ice consumption, ice pressure, and friction between ice and concrete.

### 3.1. Concrete-Ice abrasion

Based on the concrete surface measurements using the laser sensor, the abrasion was found as the difference between the unaffected zone around the edges of the concrete samples (where ice was not in contact with concrete at all) and an abraded central band of 10 mm width (where ice was sliding on concrete for the greatest distance). The cylindrical shape of the ice sample means that the greatest sliding distance is in this central band. The same approach was used by Møen et al. [5], who measured the concrete abrasion depth mechanically. The current study uses a much greater number of data points, which increases the accuracy of the results.

The results for the average ice abrasion have a large scatter between the two parallel specimens of the same concrete quality (Fig. 3 (a)), but there is less abrasion for concrete mixes with higher compressive strength (Fig. 3 (b)). The results are therefore in line with previous findings [1] that the abrasion rate is a function of concrete compressive strength.

Fig. 3(a) shows a higher abrasion rate from 0 to 1 km than from 1 to 3 km. We interpreted the higher rate from 0 to 1 km as early-stage wear, where severe initial contact took place [21], and the lower rate of the further abrasion from 1 to 3 km as a less severe wear mode [21].

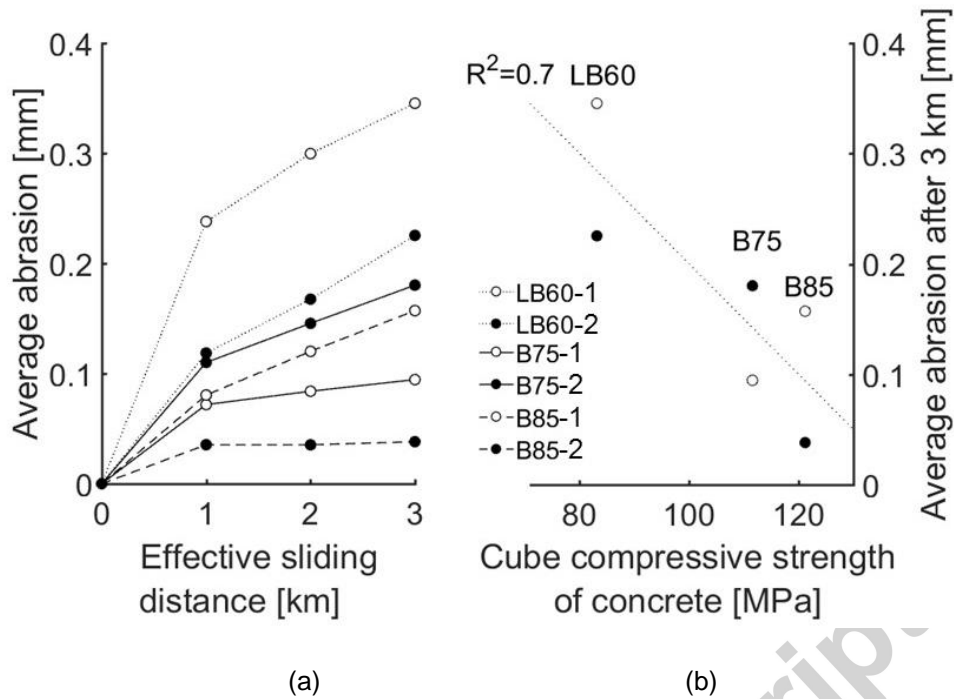


**Fig. 3.** (a) The average concrete-ice abrasion in the central band of sawn concrete surface; (b) average concrete-ice abrasion of the central band after 3 km for the various concrete mixes over the cube compressive strength of concrete at the start of concrete-ice abrasion test.

The current results are remarkably different from those from early studies of concrete-ice abrasion [22]. At that time, the results showed three stages of concrete abrasion by ice on a mould concrete surface. The first stage was interpreted as abrasion of the cement paste at the cast surface. The second (transition) stage involved a gradual reduction of wear as the coarse aggregate was increasingly exposed. Finally, a stable stage with a constant wear rate was reached with exposure of the coarse aggregate. To achieve a constant wear rate from the beginning, tests of sawn concrete surfaces were proposed [3]. It was assumed that the abrasion of a surface would be stable if 1 cm was sawn off the sample to reach a concrete depth with a constant surface area fraction of aggregate. Remarkably, the results in Fig. 3(a) show that, even with sawn concrete surfaces, there is still an

initial stage with a higher abrasion rate that cannot be explained by the three-stage model above.

The same kind of severe–mild wear transition has also been observed in wear tests of other types of material, such as uncompressed UHMWRE (ultrahigh molecular weight polyethylene) [23], iron [24–26], and carbon steel [27, 28]. Various wear modes have been found to be influenced by normal stiffness in loading (physically by normal loading) and sliding velocity[27]; the severe–mild wear transition was observed in wear tests of carbon steel at low stiffness (1-600 N/mm) and low sliding velocity (0.25 m/s). When the sliding velocity was increased to 1.57 m/s, only the severe mode was observed. The role of wear particles in severe–mild wear transition has been investigated [25, 28], and it was found that, during the severe–mild wear transition, the morphology of the wear particles also changed from coarse to fine. The attachment of oxidized fine wear particles to the surface created a protective oxide film, which induced mild wear. The severe initial wear rate of UHMWRE was interpreted as caused by nonlinear creep deformation, which then reached a steady state, creating the mild wear rate. Another interpretation of high initial wear was wear of rough machined surface. Mathematical models of abrasive wear of concrete have been developed for various exposures [12, 29]. The decreasing wear rate after the maximum wear rate is reached has been modelled and compared with ASTM C 1138 wear experiments on HPC [29]. The concrete samples with higher wear resistance reached the maximum wear rate later than samples with lower resistance properties.

### 3.2. Concrete-Ice abrasion vs. ice consumption

The role of the mating material, ice in our case, is very important. It is well-known that the harder the mating material, the higher is the abrasion of the tested material [21]. Measurements of the consumption of the mating material, however, are rare. In our case we think it is interesting since the softer ice is capable of wearing the harder concrete.

Fig. 4(a) shows the accumulated ice consumption versus the accumulated concrete abrasion for the same test series as in Fig. 3(a). Each marker represents 1, 2 or 3 kilometres of the effective sliding distance of ice passing a point on the concrete surface along the central band. For a constant ice-sliding distance of 3 km, the accumulated ice consumption varied a lot between the 6 specimens. The ice consumption was in the order of 30,000–100,000 times greater than the wear of the concrete, so the concrete is clearly a very durable material considering that the differences between concrete and ice in mechanical properties such as strength and elastic modulus are rather small: in the order of only 1–10 times greater for concrete than for ice.

The ratio in Fig. 4(b) shows that the higher concrete abrasion rate during the first kilometre already visible in Fig. 3(a) is accompanied by a relatively low ice consumption rate. For all six series the ratio of the concrete abrasion rate to the ice consumption rate decreases substantially in the subsequent sliding distance intervals.

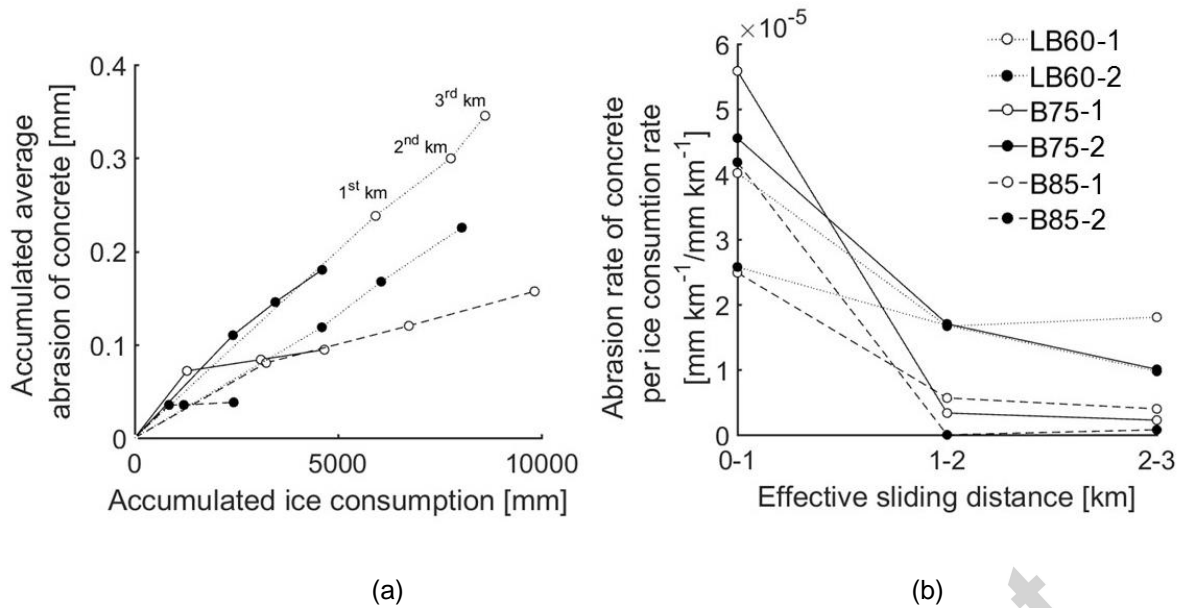


**Fig. 4.** (a) The accumulated average concrete-ice abrasion vs. the accumulated ice consumption, with each marker representing a kilometre of sliding distance; (b) the ratio of the concrete abrasion rate and the ice consumption rate for three contiguous sliding distances of 1 km.

One possible explanation for the varying ice consumption could be differing fracture modes of the ice. As a simplification, we could say that there are two extremes in contact between ice and a concrete surface: sliding and crushing. Our test set-up was originally designed for testing sliding. The ice sample in our machine is unconfined in the tight ice sample holder during the test, because the ice was constantly pushed through the ice sample holder. This meant that our machine could not simulate the crushing of ice. To improve the possibility of varying the ice loading mode, a spallation-sliding mode was developed by giving the sliding ice less lateral support (and therefore less confinement) from the steel ice-holder (Fig. 2) using a relatively simple method [11]. This was termed spallation and resulted in large amounts of ice debris and much greater ice consumption than the sliding mode, which in turn was found to affect the wear of the concrete [11].

### 3.3. Ice consumption

Ice consumption can be seen as an ice exposure parameter. As mentioned above, it was earlier observed that there is a relationship between the abrasion of concrete and the type of ice damage. So the scatter in concrete abrasion between two identical concrete specimens made from the same concrete mix is probably, at least partly, due to the substantially greater scatter in ice fracture [30] than in concrete fracture. The average coefficient of variation in the cube compressive strength of the concrete was 1.2%, the average coefficient of variation in the concrete abrasion was 53.9%, and the average coefficient of variation in the ice consumption was 101.8%.

Fig. 5 shows that the frequency distribution of the ice consumption during the test varied widely and was not concentrated. Most of the ice for all 6 concrete specimens was consumed at rates lower than 2000 mm/km. The two LWC (lightweight concrete) samples LB60-1 and LB60-2 both consumed a large number of ice cylinders at very high ice consumption rates of around 9000 mm/km. These were also the two concrete specimens that gave the highest average concrete abrasion in Fig. 3. On the other hand, the two concrete specimens with the lowest abrasion and highest strength, B85-1 and B85-2, consumed comparatively few ice cylinders with a high ice consumption rate. The two concrete specimens with the lowest abrasion, B75-1 and B85-2, consumed few or no ice cylinders at very a high ice consumption rate. From this, it seems that, at least qualitatively, there is a tendency for a temporarily high ice consumption to cause high concrete abrasion.

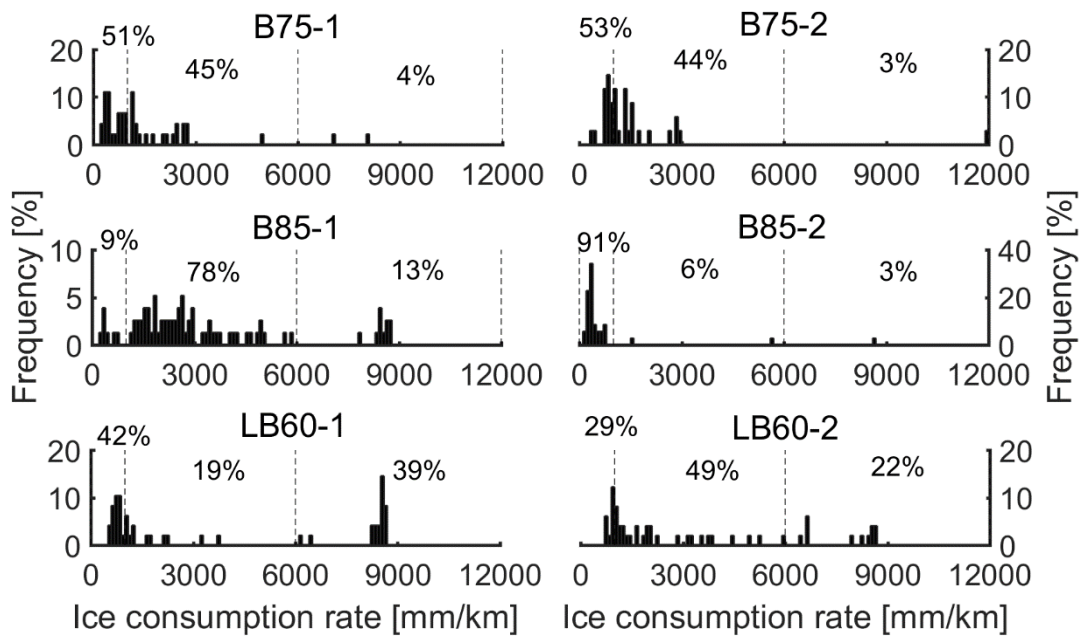


**Fig. 5.** Frequency distribution of the ice consumption during the test (using 120 bins of size 100 mm/km).

### 3.4. Effect of ice consumption on COF in two characteristic cases

Fig. 6 shows the variation in the ice consumption rate over the 3 km of ice sliding on concrete specimen B75-1 for the 45 ice cylinders used on it. The ice consumption varies greatly and seemingly randomly, from a few hundred mm of ice per km of sliding to more than 8000 mm of ice per km of sliding.

A closer look at the time series of various ice specimens sliding over concrete specimen B75-1 can be made by comparing two ice cylinders in Fig. 6: the one with an ice consumption rate of 2474.7 mm/km (Case 1) and the one with an ice consumption rate of 679.35 mm/km (Case 2). Since the difference in ice consumption rate is possibly related to concrete-ice abrasion, it is interesting to look at other exposure parameters for Case 1 and Case 2. We therefore investigated the

ice pressure, the velocity, and the coefficient of friction between the ice and concrete.

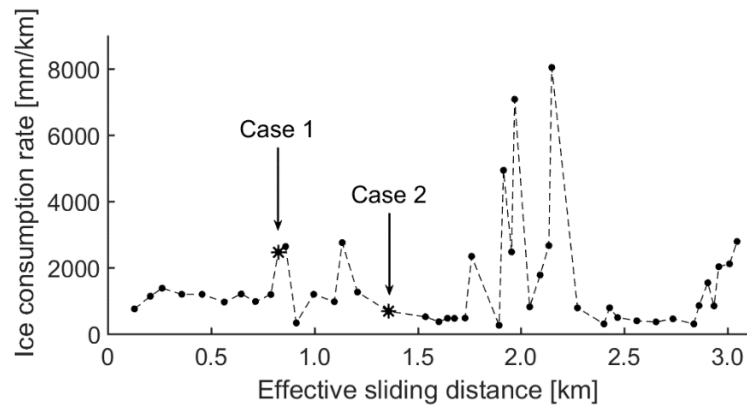


**Fig. 6.** Variation in ice consumption with sliding distance for sample B75-1

#### 3.4.1. Nominal ice pressure for Case 1 and Case 2

Fig. 7 shows the nominal ice pressure over time for each of the two cases. The time is limited by the length of the ice sample: 188 mm for Case 1 and 193 mm for Case 2. In Case 1, the ice sample was consumed in approx. 600 seconds, whereas in Case 2, the ice sample was consumed in approx. 2700 seconds.

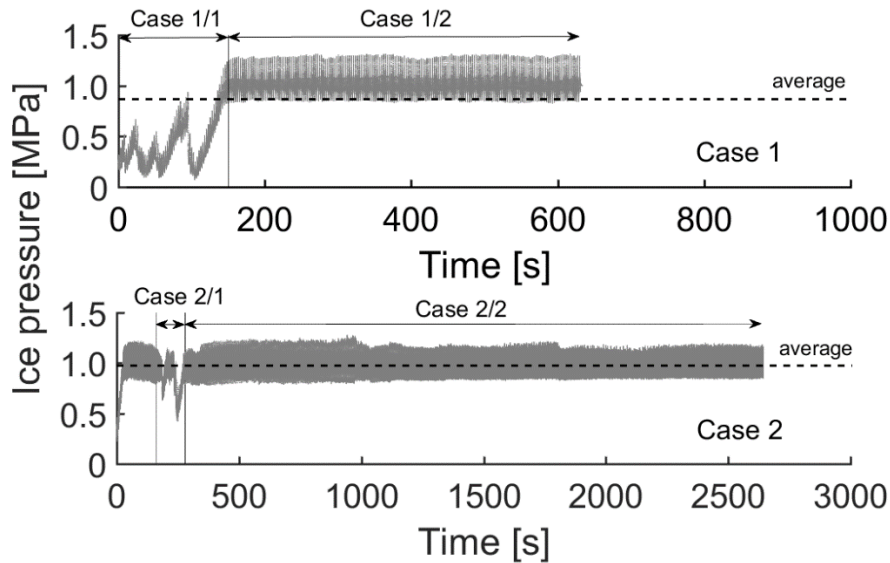


**Fig. 7.** The ice pressure in Cases 1 and 2 with differing ice consumption

The variation of the ice pressure is contradictory to the fact that the loading during the test was constant. Figure 7 demonstrates two types of pressure instability. The first one is a cyclical fluctuation of ice pressure which is addressed to ice position and gain of the feedback system, it goes up and down when the machine is going back and forth. This can be seen in Fig. 7 (marked as Case 1/2 and Case 2/2). The standard deviation of ice pressure induced by this fluctuation is 0.07 MPa. The second type is a large drop in the nominal ice pressure during the test (marked as Case 1/1 and Case 2/1). Such pressure drops give the standard deviation of 0.28 MPa and 0.09 MPa for Case 1 and Case 2 respectively.

The large drop in the nominal ice pressure was interpreted as the pulverisation of the ice sample due to a high concentration of cracks [11] during the spallation process, that demonstrates the brittle behaviour of ice. The spallation was provoked by giving less lateral support to the lower part of the ice cylinder in sliding contact with the concrete by increasing the gap between the concrete surface and the supporting steel cylinder to 8 mm [11]. When the ice sample could no longer

withstand the target load it spalled, and both the stiffness of the loading system and the gain of the control system were not able to suppress such unstable behaviour causing the load to drop rapidly (Fig. 7). This is considered as a dilemma of control: if the machine would have been controlled in such a way that these load drops would have been circumvented, we would possibly face unwanted local and global inertia effects. In the used set-up, this feature of the machine response limits the possibility to study the real contact interaction between ice and concrete. We expressed the ice pressure as a ratio of nominal load and ice cross section, with an assumption that the contact area is constant. However, the contact area is always smaller than an apparent area [31]. Moreover, the brittle fracture of the ice sample at Case 1/1 created an irregular ice surface in contact with the concrete, which is smaller than the original surface (Fig. 8 (a)). In contrast, during the sliding in Case 2, the ice sample was flat in contact with the concrete (Fig. 8 (b)), and gradual spallation took place around the edges of the ice sample. It means that although the average pressure drops in Fig.7, the contact pressure in the contact zone between the concrete surface and sharp ice asperities could increase due to decreasing of the contact area. Since the pressure distribution is not uniform, such high stress concentrations due to the brittle behaviour of ice are known as high-pressure zones (HPZ) [32]. The HPZs appear and disappear rapidly with the brittle behaviour of ice [33]. Hypothetically, the lowest pressure in Fig. 7 (which is 0.1 MPa) could be distributed over 5% or 1% of the apparent area for a few seconds that will give 2 MPa or 10 MPa of ice pressure in potential HPZ. Such great local increase in contact pressure can induce local degradation of the concrete surface. However, we are aware that the origin of HPZ is strongly affected by high confinement of ice floe, which is hard to simulate in our concrete-ice abrasion test. The spallation and

pulverisation of ice during sliding tests produces ice fragments of various sizes (Fig. 8 (c)). These ice wear particles are much greater than the magnitude of concrete-ice abrasion. The sharp shape of the ice fragments highlights the possibility of HPZs appearance.

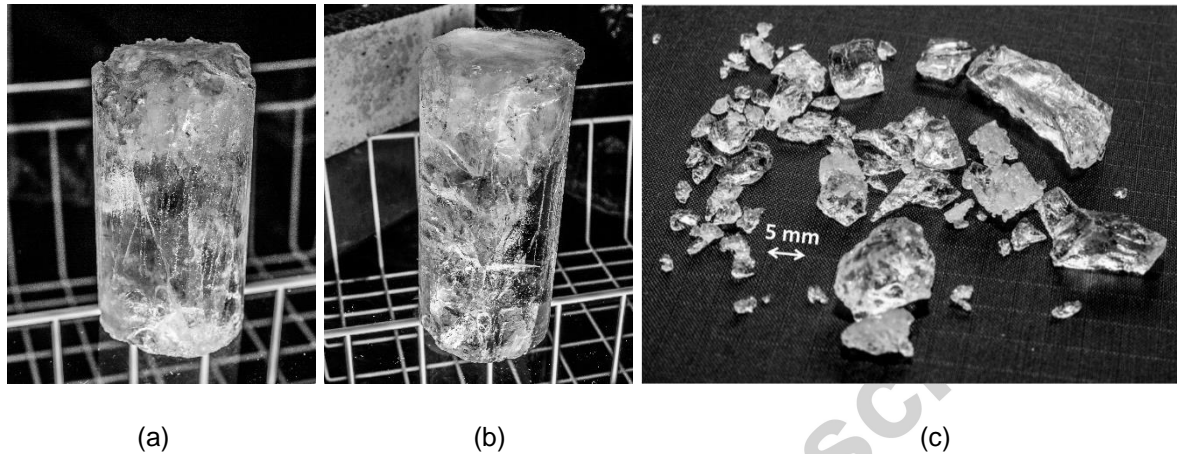


**Fig. 8.** (a) Typical ice sample for Case 1/1, (b) typical ice sample for Cases 1/2 and 2/2, (c) ice fragments after spallation during a sliding test.

### 3.4.2. *COF vs. sliding velocity*

Fig. 9 shows the distribution of the Coefficient of Friction (COF) over the sliding velocity for Cases 1/1, 1/2, 2/1 and 2/2 as shown in Fig. 7. The COF was derived as the ratio between the responses of the horizontal and vertical load cells. The velocity was derived as the ratio between the logged changes in position and time, and it varied from 0 to 0.3 m/s. To make it possible to detect any asymmetry in the machine movement, all results were plotted separately for forward and backward sliding directions. If we compare the left-hand and right-hand plots in Fig. 9, there appears to be no clear difference between the two opposite directions. The dependence of the COF on the sliding velocity for arbitrary mating materials is the

subject of ongoing research, and higher-order dependencies might yet be revealed [34]. The solid lines in Fig. 9 are fourth-power polynomial functions of the COF over the sliding velocity.

Fig. 9 shows that the COF depends on the sliding velocity. The maximum COF corresponds to a velocity approaching zero. Remarkably, the COF during pulverisation events (Fig. 7 Case 1/1) was very high (0.29–0.26) compared to the COF for the rest of the time series (0.096–0.10) (Fig. 7, Case 1/2). There was also a difference in the COF between Case 2/1 and Case 2/2; it was 0.09 and 0.06 respectively at a velocity close to zero for the forward sliding direction. The difference was not as clear as in Case 1; this might be due to the smaller load-changing amplitude in Case 2 (Fig. 7, Case 2).

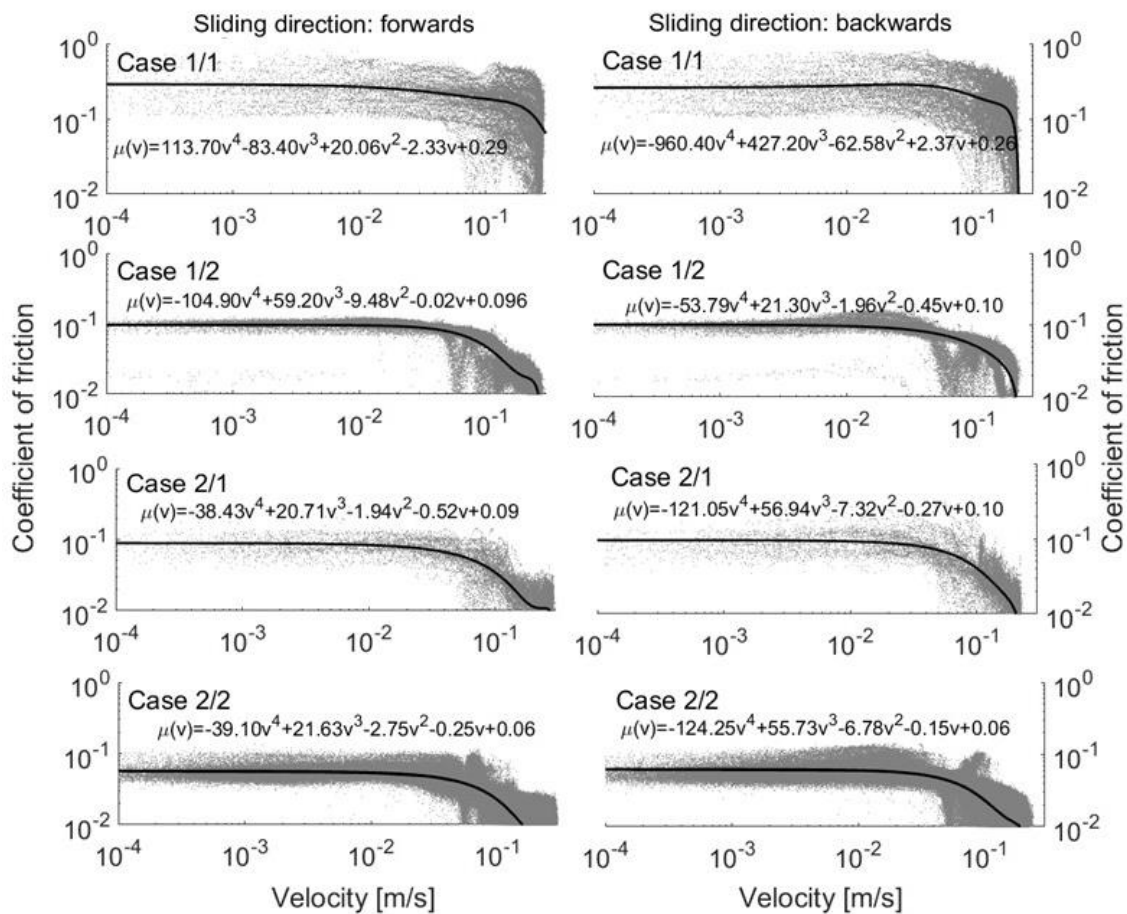
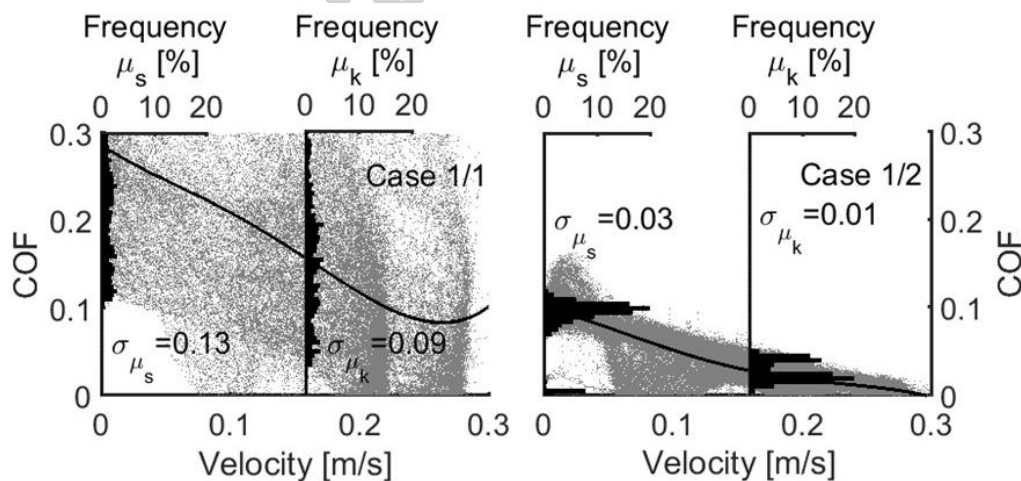


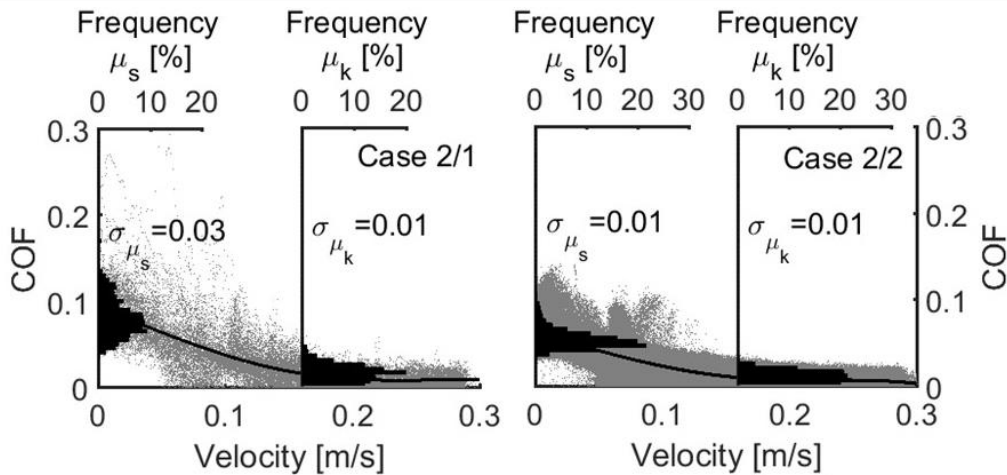
**Fig. 9.** The variation in the coefficient of friction over the velocity for different loading cases: Case 1/1, Case 1/2 and Case 2/1 and Case 2/2 (Fig. 7) for forward and backward sliding directions.

### 3.4.3. Static and kinetic COF

Fig. 10 shows the same data as in Fig. 9 for Case 1 and 2, limited to COF = 0.3 on the y-axes and plotted as frequency distributions of the coefficient of static and kinetic friction. The coefficient of static friction was found for the velocity range of 0–0.005 m/s, and the coefficient of kinetic friction was found for the velocity range of 0.158–0.163 m/s, where the kinetic friction corresponds to the average sliding velocity of the entire sinusoidal movement cycle. The solid lines in Fig. 10 are fourth-power polynomial functions of the COF over the sliding velocity. The frequency distributions show a concentration of data clouds close to the polynomial regression functions.



(a)



(b)

**Fig. 10.** The frequency distribution of the static and kinetic coefficient of friction: (a) Case 1/1 and 1/2; (b) Case 2/1 and 2/2 (bin range 0:0.005:1).

The range of the COF measured was relatively large and went beyond 0.3. The standard deviation is different for static and kinetic friction and is plotted in Fig. 10. The results show that the COF values obtained during pulverization events with unstable load (Case 1/1 and Case 2/1) were statistically different from those measured with stable-load sliding. Such short random periods with high ice consumption, such as Case 1/1 and Case 2/1 where ice spallation into fragments occurs (Fig. 8 (c)), are rare compared to the majority of the time series. The majority seems to be dominated by sliding, but spallation probably affects the wear. Hypothetically, the short contact of sharp ice fragments with the concrete surface could cause the onset of severe wear or pull-out of wear particles. Wear particles such as cement paste or fine aggregates like quartz could stay in the contact zone as third-body wear and initiate further damage.

### 3.4.4. Pressure distribution and COF

Fig. 11 shows the frequency distribution of the ice pressure (solid line) and the corresponding COF (grey point cloud). As mentioned above, the cloud of COF measurements has a low density at low pressure, and the main concentration of events is around the target load 1MPa. The low values for the ice pressure during the test are due to ice spallation and the resulting high ice consumption. Both cases show that the highest values of COF correspond to lower ice pressure. As was mentioned above, in Section 3.4.1., the drop of the nominal ice pressure in this experiment does not exclude the chance of HPZs formation at the same time. In this case, the highest values of COF could correspond the HPZs.

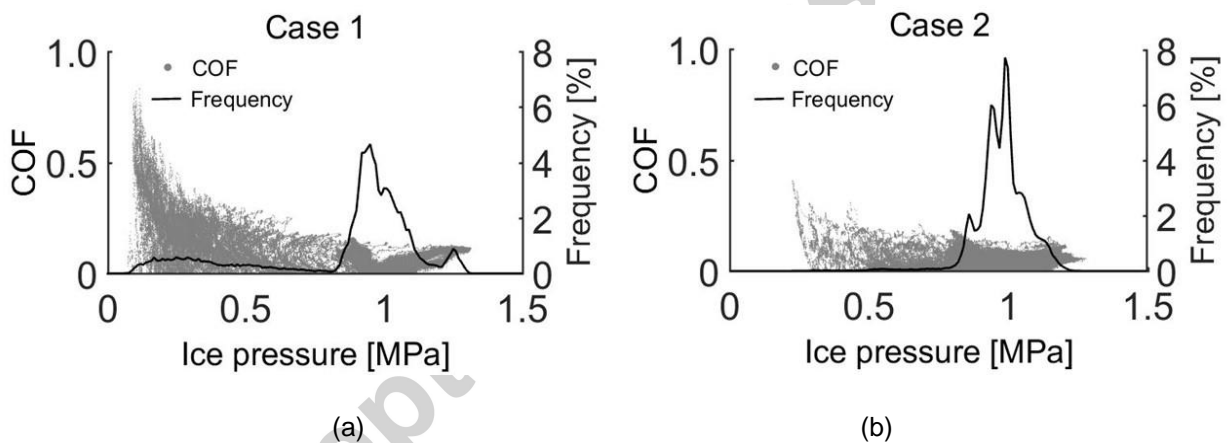


**Fig. 11.** The distribution of the COF over the ice pressure (grey markers), and the frequency distribution of the ice pressure (solid line): (a) for ice consumption 2474.7 mm/km; (b) for ice consumption 679.4 mm/km (bin ranges 0:0.01:1.5).

### 3.5. Abrasion rates in different areas on the concrete surface

Fig. 12 shows the abrasion rates for three different areas of the central band of the concrete surface: the left-hand, central and right-hand parts of the abraded surface (see the insert in Fig. 12). The effective sliding distance depends on the circular shape of the ice in the contact area, and it is shorter at both ends of the central band and where the ice sample stops moving. This means that the abrasion rate differs in the different areas. The highest abrasion was on the right-hand side due to an eccentricity in the abrasion machine. The nominal ice pressure was also higher on the right-hand side due to same eccentricity.

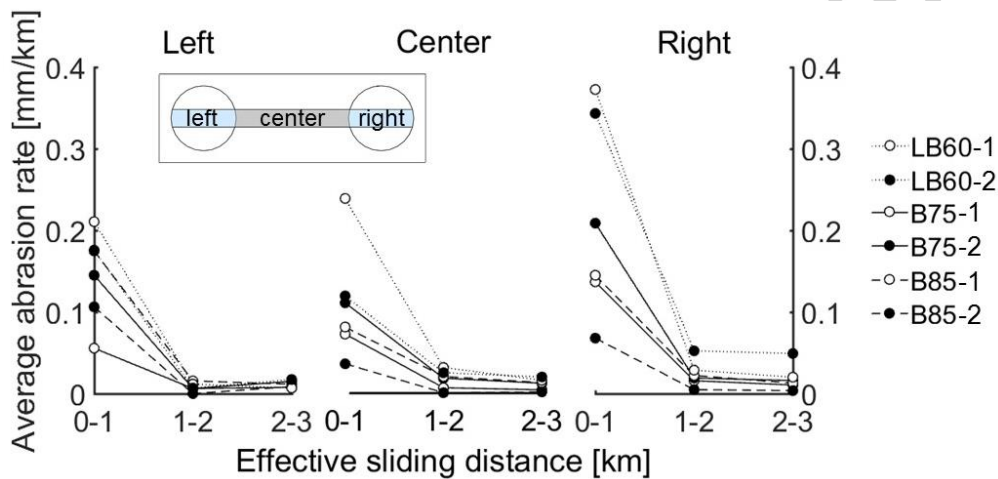


**Fig. 12.** The concrete abrasion rate in different areas and with different sliding distances.

### 3.6. The abrasion rate vs. the coefficient of friction

Fig. 13 shows the COF vs. the abrasion rate of the concrete for the initial wear in the first 1 km of effective sliding distance and for the mild wear from the next 2 km of effective sliding distance. To make it possible to compare the COF with the abrasion rate, we use the average COF per 1 km of effective sliding distance. Fig. 13 shows that the average COF concentrated in the static (0-0.01) and kinetic (0.05-0.10)

regions, and the resulting average COF shows no clear relationship to the abrasion rate in the actual areas. Possibly the amount of data for friction and wear are too limited in each small area at the centre and ends of the central band shown inserted in Fig. 12. This small-scale effect of the concrete-ice abrasion measurement is probably typical for many of the effects where we see high scatter in our experiment and underlines the general difficulty of simulating the complex concrete-ice abrasion process by a limited experiment.

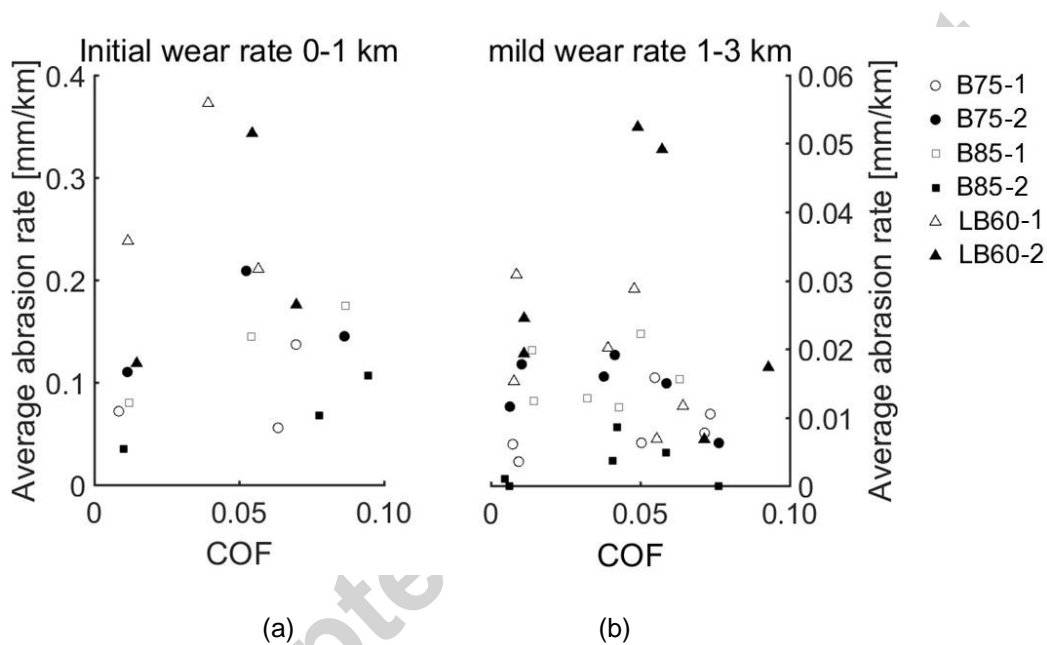


**Fig. 13.** The coefficient of friction and the average abrasion rate for: (a) initial wear, from 0 to 1 km of effective sliding distance; and (b) mild wear from 1 to 3 km.

#### 4. Conclusions

Based on the measurements of three quantities (ice consumption, ice pressure and friction between ice and concrete), we came to the following conclusions:

- The abrasion of high performance concrete after 3 km of effective sliding distance is low (in the order of 0.1 mm).

- Concrete-ice abrasion is higher for concrete mixes with lower cube compressive strength, as expected.
- Concrete-ice abrasion changes from severe (from 0 to 1 km) to mild (from 1 to 3 km) wear, even when the test surfaces are sawn.
- Ice consumption during concrete-ice abrasion testing is a randomly varying parameter associated with the much greater scatter in ice fracture properties than in concrete fracture properties.
- High ice consumption due to ice spallation and pulverization during the test seems to affect concrete ice abrasion.
- The COF is higher during ice spallation and pulverization due to the rough surface of the ice.
- The COF is not directly correlated to the abrasion.
- The wear of ice is 30,000 – 100,000 times larger than the wear of concrete in spite of that the strength and stiffness of the concrete is only in the order 1 – 10 times that of ice.

## Acknowledgments

This research formed part of the DaCS (Durable advanced Concrete Solutions) project. The financial contribution of the Norwegian Research Council and the partners is gratefully acknowledged. The DaCS project partners are: Kværner AS (project owner), Axion AS (Stalite), AF Gruppen Norge AS, Concrete Structures AS, Mapei AS, Multiconsult AS, NorBetong AS, Norcem AS, NPRA (Statens Vegvesen), Norges Teknisk-Naturvitenskapelige Universitet (NTNU), SINTEF Byggforsk, Skanska Norge AS, Unicon AS and Veidekke Entreprenør AS.

The authors also wish to thank PhD Sønke Maus in the department of Civil and Environmental Engineering for the ice density and porosity calculations based on X-ray micro-computed tomography, and our colleague, PhD Giedrius Zirgulis in the department of Structural Engineering, NTNU, for the photographs.

## References

- [1] S. Huovinen, Abrasion of concrete structures by ice, *Cement and Concrete Research* 23 (1) (1993) 69–82.
- [2] A.T. Bekker, T.E. Uvarova, E.E. Pomnikov, A.E. Farafonov, I.G. Prytkov, R.S. Tyutrin, Experimental study of concrete resistance to ice abrasion, in *Proceedings of the 21st International Offshore and Polar Engineering Conference*, 2011.
- [3] M. Hanada, M. Ujihira, F. Hara, H. Saeki, Abrasion rate of various materials due to the movement of ice sheets, in *Proceedings of the 6th International Offshore and Polar Engineering Conference*, 1996.
- [4] B. Fiorio, Wear characterisation and degradation mechanisms of a concrete surface under ice friction, *Construction and Building Materials* 19(5) (2005) 366–375.
- [5] E. Møen, K.V. Høiseith, B. Leira, K.V. Høyland, Experimental study of concrete abrasion due to ice friction – Part I: Set-up, ice abrasion vs. material properties and exposure conditions, *Cold Regions Science and Technology* 110 (2015) 183–201.
- [6] J. Tijssen, S. Bruneau, and B. Colbourne, Laboratory examination of ice loads and effects on concrete surfaces from bi-axial collision and adhesion events, in *Proceedings of the International Conference on Port and Ocean Engineering under Arctic Conditions, POAC*, 2015.
- [7] Y. Itoh, Y. Tanaka, A. Delgado, H. Saeki, Abrasion depth distribution of a cylindrical concrete structure due to sea ice movement, *International Journal of Offshore and Polar Engineering* 6 (2) (1996) 144–151.

- [8] F. Hara, H. Saeki, M. Sato, Y. Takahashi, H. Tachibana, Prediction of the Degree of Abrasion of Bridge Piers by Fresh Water Ice and the Protective Measures, in Proceedings of the Concrete Under Severe Conditions Environment and Loading. (1995) 482-494.
- [9] E. Møen, K.V Høiseth, B. Leira, K.V. Høyland, Experimental study of concrete abrasion due to ice friction - Part II: Statistical representation of abrasion rates and simple, linear models for estimation. Cold Regions Science and Technology 110 (2015) 202-214.
- [10] S. Løset, K. Shkhinek, K.V. Høyland, *Ice Physics and Mechanics*, NTNU, 1998.
- [11] G. Shamsutdinova, M.A.N. Hendriks, S. Jacobsen, Concrete-Ice Abrasion Test with Sliding Ice and Ice Spallation, Nordic Concrete Research 57 (2017) 39–57.
- [12] S. Jacobsen, G.W. Scherer, E.M. Schulson, Concrete-ice abrasion mechanics, Cement and Concrete Research 73 (2015) 79–95.
- [13] G.W. Stachowiak, A.W. Batchelor, Engineering tribology, Amsterdam 3rd edition (2005)
- [14] R. Cepuritis, Physical properties of Norwegian mineral fillers investigated by different methods, COIN Project report 43 (2012).
- [15] EN 12350-1, Testing fresh concrete. Sampling, 2009.
- [16] EN 206:2013+NA:2014, Concrete – Specification, performance, production and conformity – National annex, 2014.
- [17] A. Pustogvar, A. Kulyakhtin, Sea ice density measurements. Methods and uncertainties, Cold Regions Science and Technology 131 (2016) 46–52.
- [18] P.V. Hobbs, Ice physics, Oxford: Clarendon Press, 1974
- [19] S. Maus, J. Becker, S. Leisinger, A. Wiegmann, Oil saturation of the sea ice pore space, in Proceedings of the International Conference on Port and Ocean Engineering under Arctic Conditions, POAC, 2015.
- [20] E.M. Schulson, P. Duval, Creep and Fracture of Ice (2009).
- [21] G.W. Stachowiak, Wear: materials, mechanisms and practice, 2005.

- [22] Y. Itoh, A. Yoshida, M. Tsuchiya, K. Katoh, K. Sasaki, H. Saeki, An experimental study on abrasion of concrete due to sea ice. In: OTC 88 Proceedings 20th Annual Offshore Technology Conference 1988, pp. 61–68.
- [23] K.-Y. Lee, D. Pienkowski, Reduction in the initial wear of ultrahigh molecular weight polyethylene after compressive creep deformation, *Wear* 203–204 (1997) 375–379.
- [24] K.i. Hiratsuka, M. Inagaki, Effects of temperature, sliding velocity and non-friction time on severe-mild wear transition of iron. *Tribology International* 49 (2012) 39–43.
- [25] K.i. Hiratsuka, K.i. Muramoto, Role of wear particles in severe–mild wear transition, *Wear* 259 (1–6) (2005) 467–476.
- [26] H. Kato, Effects of supply of fine oxide particles onto rubbing steel surfaces on severe–mild wear transition and oxide film formation, *Tribology International* 41 (8) (2008) 735–742.
- [27] Y.C. Chiou, K. Kato, T. Kayaba, Effect of Normal Stiffness in Loading System on Wear of Carbon Steel – Part 1: Severe-Mild Wear Transition, *Journal of Tribology* 107 (4) (1985) 491–495.
- [28] A. Iwabuchi, H. Kubosawa, K. Hori, The dependence of the transition from severe to mild wear on load and surface roughness when the oxide particles are supplied before sliding, *Wear*, 139 (2) (1990) 319–333.
- [29] E. Horszczaruk, Mathematical model of abrasive wear of high performance concrete. *Wear* 264 (1) (2008) 113–118.
- [30] E.M. Schulson, The brittle compressive fracture of ice, *Acta Metallurgica et Materialia* 38 (10) (1990) 1963–1976.
- [31] B. Basu, M. Kalin, *Tribology of Ceramics and Composites. Materials Science Perspective. Tribology properties of ceramics and composites.* 2011.
- [32] I.J. Jordaan, Mechanics of ice-structure interaction. *Engineering Fracture Mechanics* 68 (17-18) (2001) 923-1960.

- [33] G.W. Timco, D. Sudom, Revisiting the Sanderson pressure–area curve: Defining parameters that influence ice pressure. *Cold Regions Science and Technology* 95 (2013) 53-66.
- [34] O.M. Braun, M. Peyrard, Dependence of kinetic friction on velocity: Master equation approach. *Physical Review E* 83 (4) (2011) 046129-1-9.

### Highlights

- Simultaneous measurements of concrete wear, ice consumption and friction 1 were made. 2
- The observed abrasion was very low: maximum 0.35 mm after 3 km. 3
- Severe-to-mild wear transition of concrete-ice abrasion was observed. 4
- Ice spallation increases ice consumption and coefficient of friction.